Received: 8 August 2016 | Accepted: 19 December 2016
DOI 10.1002/hyp.11115

WILEY

RESEARCH ARTICLE

Improving runoff prediction using agronomical information in a cropped, loess covered catchment

Marie Lefrancq[1] | Paul Van Dijk[2] | Victor Jetten[3] | Matthieu Schwob[1] | Sylvain Payraudeau[1]

[1] Laboratory of Hydrology and Geochemistry of Strasbourg (LHyGeS), University of Strasbourg/ENGEES, CNRS, 1 rue Blessig, F-67084 Strasbourg CEDEX, France

[2] Association pour la Relance Agronomique en Alsace (ARAA), 2 rue de Rome 67300 Schiltigheim, France

[3] Faculty of Geo-Information Science and Earth Observation ITC, University of Twente, Enschede, The Netherlands

Correspondence
Sylvain Payraudeau, Laboratory of Hydrology and Geochemistry of Strasbourg (LHyGeS), University of Strasbourg/ENGEES, CNRS, 1 rue Blessig, F-67084 Strasbourg CEDEX, France
Email: sylvain.payraudeau@engees.unistra.fr

Abstract

Predicting runoff hot spots and hot-moments within a headwater crop-catchment is of the utmost importance to reduce adverse effects on aquatic ecosystems by adapting land use management to control runoff. Reliable predictions of runoff patterns during a crop growing season remain challenging. This is mainly due to the large spatial and temporal variations of topsoil hydraulic properties controlled by complex interactions between weather, growing vegetation, and cropping operations. This interaction can significantly modify runoff patterns and few process-based models can integrate this evolution of topsoil properties during a crop growing season at the catchment scale. Therefore, the purpose of this study was to better constrain the event-based hydrological model Limburg Soil Erosion Model by incorporating temporal constraints for input topsoil properties during a crop growing season (LISEM). The results of the temporal constraint strategy (TCS) were compared with a classical event per event calibration strategy (EES) using multi-scale runoff information (from plot to catchment). The EES and TCS approaches were applied in a loess catchment of 47 ha located 30 km northeast of Strasbourg (Alsace, France). A slight decrease of the Nash–Sutcliffe efficiency criterion on runoff discharge for TCS compared to EES was counterbalanced by a clear improvement of the spatial runoff patterns within the catchment. This study showed that limited agronomical and climatic information added during the calibration step improved the spatial runoff predictions of an event-based model. Reliable prediction of runoff source, connectivity, and dynamics can then be derived and discussed with stakeholders to identify runoff hot spots and hot-moments for subsequent land use and crop management modifications.

KEYWORDS

calibration, equifinality, hot spot, Manning's coefficient, saturated hydraulic conductivity, soil surface characteristics

1 | INTRODUCTION

Runoff is the main driver of soil losses (Garcia-Ruiz, Nadal-Romero, Lana-Renault, & Begueria, 2013) and nutrient (Outram, Cooper, Sunnenberg, Hiscock, & Lovett, 2016) and pesticide (Doppler, Luck, Camenzuli, Krauss, & Stamm, 2014) off-site transport in agricultural catchments with adverse effects on society (Boardman & Vandaele, 2016), biodiversity, and ecosystem functioning (Hasenbein, Lawler, Geist, & Connon, 2016). Therefore, assessing and predicting the runoff hot spots, that is, areas that contribute disproportionally to runoff, and hot-moments are of the utmost importance to control runoff through adapted land use, mitigation measures, or agricultural practices in a catchment.

Runoff hot spots in agricultural catchments are highly dynamic and largely influenced by the structural evolution of soils due to agricultural practices (Doppler et al., 2014; Pare, Andrieux, Louchart, Biarnes, & Voltz, 2011). Topsoil saturated hydraulic conductivity (K_{sat}) directly controls infiltration versus runoff partitioning with rainfall intensity (Pare et al., 2011). K_{sat} exhibits higher values after tillage and gradually decreases up to one order of magnitude due to breakdown of aggregates caused by rainfall and the clogging of larger pores, especially in silty loam soils (Chahinian, Voltz, Moussa, & Trotoux, 2006; Zeng, Wang, Zhang, & Zhang, 2013). K_{sat} can also be affected by organisms such as soil fauna (Capowiez et al., 2009) and biological crusting (Rodriguez-Caballero, Canton, & Jetten, 2015). The runoff connectivity is controlled by K_{sat} patterns (Harel & Mouche, 2014), as well as by

macrotopography, for example, berms, embankments, ditches (Levavasseur, Bailly, Lagacherie, Colin, & Rabotin, 2012), hedges (Gascuel-Odoux et al., 2011), detention ponds (Chrétien, Gagnon, Thériault, & Guillou, 2016), and by microtopography resulting from tillage or wheel tracks (FpMasters, Rohde, Gurner, & Reid, 2013). The runoff dynamic, that is, the flow discharge, is controlled by the slope, the surface roughness and the hydraulic resistance expressed by the Manning's coefficient (n). During a growing season, rainfall events are expected to progressively smooth the soil roughness after tillage while crop growth maintains and increases hydraulic resistance (Li & Zhang, 2001). Knowledge and understanding of spatial heterogeneity and temporal dynamics of soil surface and hydrodynamic characteristics is therefore crucial for predicting runoff in agricultural catchments.

However, after 50 years of process-based model developments (Fatichi et al., 2016; Freeze & Harlan, 1969), even if temporal variations of topsoil properties during a growing season are known, few process-based models integrate them at the catchment scale. Continuous physically-based hydrological models such as CATchment HYdrology (Muma, Gumiere, & Rousseau, 2014), MIKE-SHE (Zhang, Madsen, Ridler, Refsgaard, & Jensen, 2015), or Soil & Water Assessment Tool (Her, Chaubey, Frankenberger, & Smith, 2016) can provide runoff patterns, connectivity, and dynamics but only with fixed K_{sat} and n values for each soil-land use combination for an entire season. Continuous models are not usually designed to predict the runoff from single events and generally lack sufficient spatial and temporal details (Yin et al., 2016). They are generally not suitable to describe soil erosion with sufficient detail within small catchments (Pandey, Himanshu, Mishra, & Singh, 2016). On the contrary, the strength of the event-based models is their ability to address runoff-infiltration and soil erosion processes on a physical basis at the catchment scale at high spatial and temporal resolution (Pandey et al., 2016; Starkloff & Stolte, 2014).

Event based models need to be properly initialised for each event. The estimation of soil moisture, K_{sat}, and n requires external information (Berthet, Andreassian, Perrin, & Javelle, 2009; Tramblay et al., 2010) or a calibration step for each rainfall–runoff event (Baartman, Jetten, Ritsema, & de Vente, 2012; Cuomo, Della Sala, & Novita, 2015; Kalantari et al., 2015), which may jeopardize the predictive capacity of the model. In a landscape with many land uses, calibration steps may also hamper the selection of a unique set of spatial parameters that best describe the catchment dynamics and may lead to "equifinality" as a result of over-parameterisation (Beven, 2006; Kirchner, 2006). Thus, providing process-based models with relevant agronomical data before calibration still remains a challenge. As an example, significant development in the event-based model STREAM, proposed using expert-based tables to initialise K_{sat} values depending on crop cover and crusting stage (Evrard et al., 2009). Unfortunately, the expert-based approach may reduce the model's ability to transfer to other catchments (Evrard et al., 2009). Temporal rules for including changing topsoil properties during a crop growing season are needed to improve the prediction of runoff patterns, connectivity, and dynamics at the event scale.

Therefore, the purpose of this study was to properly initialise a hydrological event-based model during a growing season and to determine rules (or constraints) for future modelers to decide which parameters need to be calibrated and how. These constraints were developed to explicitly integrate links between crop management techniques and variability of soil surface properties over time. The results of the temporal constraint strategy (TCS) were compared with a classical event per event calibration strategy (EES). Both calibration strategies were performed with the nonlinear "Parameter ESTimation" (PEST) package (Mbonimpa et al., 2015) on the event based hydrological model Limburg Soil Erosion Model (LISEM) (Baartman et al., 2012). The EES and TCS approaches were applied to a 47 ha catchment located 30 km northeast of Strasbourg (Bas-Rhin, France). The improvement of predictions was assessed for the spatial runoff patterns and connectivity using multi-scale runoff information at the outlets of a 77 m^2 plot, a 6 ha upstream subcatchment and the 47 ha catchment.

2 | MATERIAL AND METHODS

2.1 | Site description

The 47 ha catchment is located 30 km northeast of Strasbourg (Bas-Rhin, France). The mean annual temperature is 11.7°C, with a mean annual rainfall of 605 mm (±141 mm) and evapotranspiration of 820 mm (±28 mm) (2005–2011, Meteo France station in Waltenheim sur Zorn, 7 km from the study site). The slope varies slightly with a mean of 5.7% ± 2.9%, with 3.7% of the catchment surface with a slope between 0 and 2%, 37.8% with a slope between 2 and 5%, 56.4% with a slope between 5 and 10%, and 2.1% with a slope higher than 10% (Figure 1). The altitude ranges between 190 and 230 m. Water flows in open ditches to the catchment outlet (P0 in Figure 1) where it enters a 50 cm diameter pipe and flows under the road, which prevents outflow greater than 550 L s^{-1}. Since 1950, the catchment has been equipped with a tile drainage system at 80 cm depth. Only one drain outlet (Figure 1) was flowing during the study period. No flow was observed in the other drain outlets during the study period. Arable land (88%) dominates the catchment, which was planted in corn (68%), winter wheat (16%), and sugar beet (4%) as the principal crops in 2012. The road network is 3.5% of the catchment surface divided into dirt roads (1.2%), grass roads (1.7%), and paved roads (0.6%).

The spatial variability of the soil was characterised by 30 surface soil samples (0–20 cm) collected in April 2011 and by six 2 m deep soil profiles collected in November 2012. The main soil type is calcareous brown earth and calcic soils on hillsides and colluvial calcic soils in the central thalweg. The grain size distributions of the soil surface within the catchment had low variation (n = 30 samples; mean ± SD in percent): clay 30.8 ± 3.9, silt 61.0 ± 4.5, and sand 8.5 ± 4.2. The soil characteristics were $CaCO_3$ 1.1 ± 1.6%, organic matter 2.16 ± 0.3%, pH KCl 6.7 ± 0.8, phosphorus 0.11 ± 0.04 g kg^{-1}, and CEC 15.5 ± 1.3 $cmol^+$ kg^{-1}. A compacted layer (plough pan) was observed at a depth between 20 and 30 cm.

Overall, the soil characteristics indicate little variability within the catchment. Information on cropping operations (types and dates) was obtained through questionnaires addressed to the five farmers within the catchment. The farmer's practices consisted in conventional tillage (plowing in winter and seedbed preparation by harrowing) and the application of chemical fertilizers and pesticides. They often shared

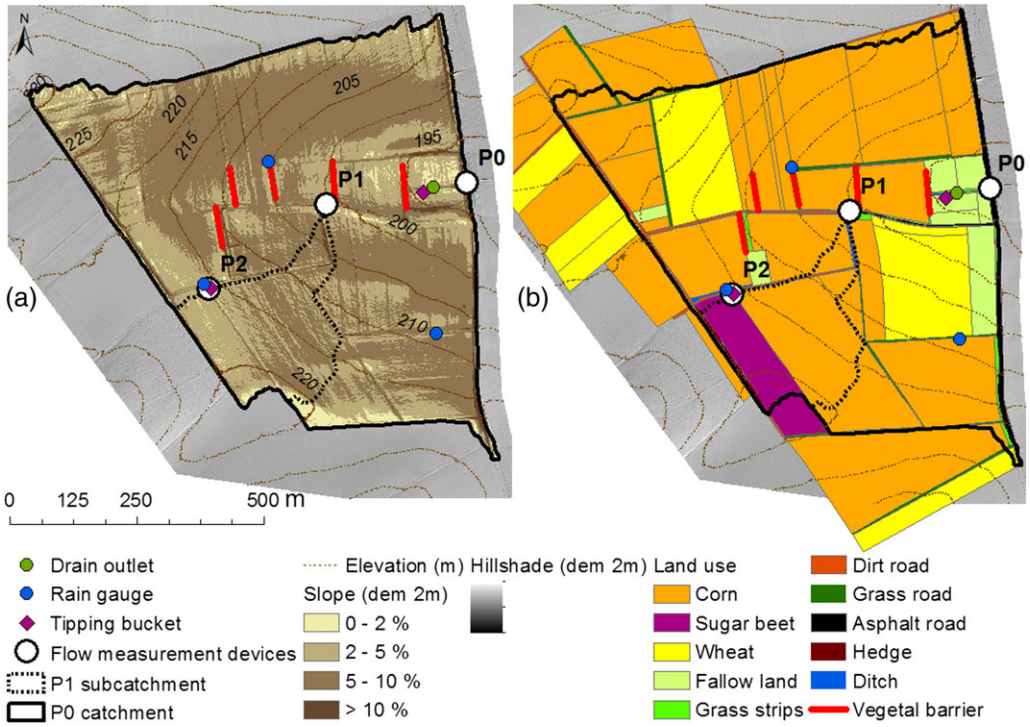

FIGURE 1 The study catchment with the experimental setup and the topography (a) and the Landuse map for 2012 (b) superimposed with the 2-m dem hillshade

the same equipment for tillage operations. None of the farmers applied conservation tillage techniques. Only one farmer applied animal manure as fertilizer every 3 years (2.5 ha, i.e., 5.3% of the catchment surface). The crop management practices (types and dates) differed between crops but very little between farmers. The study catchment was prone to significant mudflows nearly every year (Heitz, Flinois, & Glatron, 2012), and the soil was sensitive to soil crusting and compaction. In 2009, five vegetal barriers were installed in the flow path to decrease the water velocity and to retain soil particles during large events (Figure 1). Except the one furthest downslope, they have been completely filled up and aren't functional anymore and haven't been for several years. Opened ditches were also dug to move excess water rapidly to the catchment outlet. Rainfall and runoff discharges were continuously monitored between March 12 and August 14, 2012, which corresponded to the main part of the growing season for sugar beet and corn crops.

2.2 | Field measurements

The catchment was equipped with 2 tipping bucket rain gauges and 3 cumulative rain gauges (Figure 1). Based on the five rain gauges, a low spatial variation of the rainfall was observed within the catchment (±3.5 mm on a weekly basis). Therefore, the rainfall was considered to be homogeneous for the event-based simulation. Water discharge was measured at 3 nested scales, a 77 m^2 plot outlet (P2 in Figure 1), a 6 ha subcatchment outlet (P1), and the 47 ha catchment outlet (P0 in Figure 1) in order to better investigate runoff genesis, connectivity, and dynamics. The first detector measured discharge from a sugar beet plot in the uphill region of the catchment (P2, Figure 1) using a Venturi channel combined with an ultrasonic surface water level sensor (ISMA, Forbach, France). This provided key information on runoff activation for spring-crops (sugar beet and corn), which covered 72% of the catchment. Indeed, from March to July, sugar beet and corn emerged conjointly from bare soil to progressively cover 100% of the soil with vegetation. The second detector was installed in a pipe under a road controlling 6 ha (P1, Figure 1) using a pressure sensor data logger compensated with barometric pressure (Orpheus Mini, OTT, Kempten, Germany). Due to plot border overflowing and sedimentation in the pipe for the largest runoff events, the measuring devices at P1 and P2, respectively, were mainly used as "runoff event detector". At the catchment outlet (P0, Figure 1), a Doppler flowmeter (2150 Isco, Lincoln, Nebraska, USA) measured outflow with a precision for water volume of 3%. These 3 locations provided relevant multi-scale information on runoff genesis, connectivity, and dynamics for the subsequent model calibration step.

Each week, soil samples were collected from P2 to measure soil water content. Soil samples were collected from 20 subsections in P2 and composited. Nine rainfall events that each yielded more than 10 m^3 of runoff (runoff coefficient between 0.2 and 40.8%) at the outlet of the catchment were observed during the study period (Table 1). The first runoff event was observed on May 2 simultaneously with crusting of the topsoil. After runoff events, runoff patterns and pathways were mapped on the basis of traces such as incisions and sediment deposition. Based on the constant-slope method for hydrograph separation (McCuen, 2004), the contribution of the artificial drain (Figure 1) was quantified. This contribution was 8.59 ± 6.65% of the total discharge for the 9 major runoff events (>10 m3) and 33% for the total observation period. Soil erosion is a major problem in this catchment and has helped to focus this study

TABLE 1 Meteorological and hydrological characteristics of the 9 runoff events yielding at least 10 m^3 at the outlet of the catchment and occurring from May 2 to August 15, 2012

	Unit	May 2	May 21	May 23	June 7	June 11	June 12	July 10	July 08	July10
Rainfall amount	[mm]	16.2	54.4	3.8	10.8	5.8	10.8	12.8	11.0	6.2
Rainfall duration	[min]	179	204	29	106	20	180	30	164	41
6 min-peak rainfall intensity	[mm h^{-1}]	38	72	26	56	50	20	40	16	46
Total discharge	[m^3]	22.2	10567.9	143.6	208.0	147.6	408.3	227.4	79.0	23.2
Estimation of drainage contribution	[%]	22.5	1.5	13.7	3.5	5.3	6.2	4.8	13.3	6.5
Runoff event duration	[min]	75	413	55	98	84	193	91	179	38
Runoff coefficient	[%]	0.2	40.8	7.0	4.0	6.5	5.8	3.6	1.3	0.7
Maximum outflow	[L s^{-1}]	11.2	[b]	105.0	131.0	0.7	125.0	229.0	30.5	20.2
Peak time discharge[a]	[min]	184	[b]	27	84	19	53	34	90	10

[a]Time after beginning of rainfall event

[b]Flood retention

on runoff genesis with respect to runoff processes when rainfall exceeds infiltration capacity (Hortonian flow).

2.3 | Hydrological event-based model: LISEM

Limburg Soil Erosion Model was used for this study for 3 reasons. First, it is a process-based model, designed for event-based runoff and erosion predictions from small- to medium-sized catchments (<100 km^2). Second, LISEM was primary developed to describe agricultural landscape components with tillage directions, crusted and compacted zones and soil surface structure (Liu, Xu, & Ritsema, 2003). Finally, LISEM has been validated in various agricultural contexts and hydrological conditions (Baartman et al., 2012; Hessel, van den Bosch, & Vigiak, 2006; Hessel & Jetten, 2007; Kalantari et al., 2015; Sheikh, van Loon, Hessel, & Jetten, 2010). The theory and structure of LISEM were previously described (Baartman et al., 2012; De Roo, Wesseling, & Ritsema, 1996). Briefly, rainfall interception by vegetation is first calculated based on a canopy storage function (De Jong & Jetten, 2007). Then, the water partitioning between infiltration and runoff can be calculated by different equations depending on the data availability and objective of the simulation: Richard's equation (Kværnø & Stolte, 2012), Smith and Parlange's equation (Smith & Parlange, 1978), or Green and Ampt's equation for one or two soil layers (Kutílek & Nielsen, 1994). Here, infiltration was calculated by the Green and Ampt equations (Equation 1) because of (a) easier data requirement, (b) large existing expertise on the parametrisation, and (c) consistent results for Hortonian runoff.

$$q_{inf} = -K_{sat}\left(1 + \frac{(\psi + h)(\theta_{sat} - \theta_i)}{F}\right) \quad (1)$$

where q_{inf} is the infiltration rate [m s^{-1}], K_{sat} is the saturated hydraulic conductivity [m s^{-1}], F is the cumulative infiltration from the beginning of the event [m], ψ is the average matrix suction at the wetting front [m], h is the depth of the water layer at the soil surface [m], θ_{sat} is the saturated water content [−], and θ_i is the initial water content of the layer [−]. The maximum depression storage in the microrelief is estimated based on the random roughness index (*RR*, essentially the standard deviation of microrelief height differences in centimeter) and empirical equations from Kamphorst et al. (2000). Once the maximum depression storage is exceeded, runoff is generated. Runoff is routed over a user defined network that connects cells in 8 directions using a 1-D kinematic wave approximation based on Manning's equation for velocity (Equation 2; Chow et al., 2013).

$$\frac{\partial Q}{\partial x} + \frac{\partial}{\partial t}\left[\frac{n}{\sqrt{S}}P^{\frac{2}{3}}\right]^{0.6} = q_{sur} \quad (2)$$

where Q is the discharge [m^3 s^{-1}], n is the Manning's coefficient [$s/m^{1/3}$], S is the sine of the slope gradient [−], P is the wet perimeter [m], and q_{sur} is the infiltration surplus [m^2 s^{-1}]. In this study, LISEM refers to version 1.79 of OpenLISEM (http://blogs.itc.nl/lisem/, 2014).

2.4 | Model setup, input data, and parameters

Two Digital Elevation Models (DEM), at 0.5 and 2 m resolution, were extracted with ArcGIS 10.1 (ESRI, Redlands, United States) from airborne Light Detection And Ranging (LIDAR) measurements (8 points per m^2 with a vertical accuracy of 15 cm). For practical reasons (running time and data availability), the 2 m resolution was adopted for all the maps used by LISEM. The drainage direction extracted from a 0.5 m DEM was "burned" onto the 2 m DEM (Thomas et al., 2017), in order to account for the effects of small-sized topographic features, such as tillage furrows and ditches, on flow directions. The 2 m drainage direction was manually modified to enable the flow through the pipes under the roads at P0 and P1. Green and Ampt's equations for two layers were used to represent the layer influenced by tillage and the layer underneath. The soil profile was discretised in two layers at 0–25 and 25–175 cm (noted with subscripts 1 and 2, respectively). 1 min resolution rainfall data were obtained from the tipping bucket rain gauge near the outlet of the catchment (Figure 1) and a 10 sec time step was used for all the simulations. Ten different land uses were determined in 2012: corn, wheat, sugar beet, dirt road, asphalt road, grass road, grass strip, ditch, fallow land, and hedge.

Due to the high temporal variability of soil surface states and crop development, one common dataset for all runoff events lead to very poor modelling results (Baartman et al., 2012; Hessel, Messing, Chen, Ritsema, & Stolte, 2003). Therefore, initial values of vegetation and soil parameters of each LISEM simulation had to be estimated. Parameter values and estimation methods are detailed in Table 2 and Table 3.

TABLE 2 Description of the LISEM input parameters and their spatial and temporal discretisation for the event per event strategy (EES) and the temporal constraint strategy (TCS). "Spatialised" indicates that input parameters are discretised for each cell, "crop" that input parameters are homogeneous according to each 11 land uses and "homogeneous" that the input parameters were lumped for the catchment. "Fixed" indicates that input parameters are fixed over time, "temporally" that input parameters were fixed but may vary over time and "calibrated" indicates that the input parameters were calibrated

	Approaches Units	Spatial variation EES and TCS	Temporal variation		Method-source	
			EES	TCS	EES	TCS
Catchment morphology						
Digital elevation model		Spatialised	Fixed		Measurement (LIDAR)	
Slope		Spatialised	Fixed		Calculated based on DEM	
Local drainage direction		Spatialised	Fixed		Calculated based on DEM	
Soil surface						
RR	[cm]	Crop	Temporally		Field measurement and estimations (Potter, 1990)	
Manning		Crop				
for plot margins	[−]		Calibrated ±20%	Fixed	Table 3	Constraint 2
for corn/sugar beet	[−]		Calibrated	Calibrated	0.07–0.13	Constraint 5
for wheat	[−]		Calibrated	Calibrated	0.12–0.21	Constraint 5
Vegetation						
Landuse		Crop	Fixed		Orthophoto and field observation	
Surface Cover	[−]	Crop	Temporally		Field observations and estimations (Hunt, 1982)	
Crop height	[m]	Crop	Temporally		Field observations	
Leaf area Index	[−]	Crop	Temporally		LISEM user guide	
Infiltration						
Layer 1						
Saturated hydraulic conductivity		Crop				
for plot margins	[mm h^{-1}]		Calibrated ±20%	Fixed	Table 3	Constraint 2
for corn/sugar beet	[mm h^{-1}]		Calibrated	Calibrated	0.5–60 (LISEM user guide)	Constraint 4
for wheat	[mm h^{-1}]		Calibrated	Fixed	0.5–60 (LISEM user guide)	Constraint 3
Initial water content	[−]	Homogeneous	Calibrated ±20%		Depletion model (Kohler & Linsley,1951)	
Saturated water content	[−]	Homogeneous	Fixed: 0.42		Field measurement	
Suction at the wetting front	[cm]	Homogeneous	Calibrated	Fixed: 61.7	6–139 (de Roo et al., 1995)	Constraint 1
Soil depth	[m]	Homogeneous	Fixed: 0.25		Field observations	
Layer 2						
Saturated hydraulic conductivity	[mm h^{-1}]	Homogeneous	Fixed: 15.1		Head constant permeameter (Amoozegar et al.,1989)	
Initial water content	[−]	Homogeneous	Fixed: 0.3		pF curve: θ(Ψ) (Madsen et al., 1986)	
Saturated water content	[−]	Homogeneous	Fixed: 0.36		Sand Kaolin Box (Madsen et al.,1986)	
Suction at the wetting front	[cm]	Homogeneous	Fixed: 80.26		Saxton & Rawls, 2006	
Soil depth	[m]	Homogeneous	Fixed: 1.75		Field observations	

Note. DEM = digital elevation models; LISEM = Limburg Soil Erosion Model; RR = random roughness index.

TABLE 3 Saturated hydraulic conductivity and Manning's coefficient for plot margins

	Catchment surface [%]	Ksat [mm h^{-1}]	Manning's coefficient [−]
Grass strip	1.4	35	0.5
Dirt road	1.2	3	0.02
Grass road	1.7	5	0.05
Asphalt road	0.6	0.001	0.011
Ditch	0.2	20	0.1
Fallow land	1.6	20	0.2
Hedge	0.3	50	0.2

Except K_{sat1}, Green and Ampt parameters ($\theta_{i1,2}$, $\theta_{sat1,2}$, $\Psi_{1,2}$, $soildep_{1,2}$, K_{sat2}) were assumed to be homogeneous within the catchment. The surface parameters, that is, the vegetation parameters, *RR*, *n*, and K_{sat1} were assumed to only vary according to the crop types because spatial variation of soil types, slope and crop management techniques were limited within the catchment. Plot margins such as vegetal barriers, ditches, or roads were explicitly integrated in the 2 m land use map and parametrized (Table 3). The temporal variation of vegetation cover was calculated according to a sigmoidal curve based on the growth equation of Hunt (1982). Crop height and Leaf Area Index were estimated based on LISEM guide abacus (De Roo, Wesseling, Jetten, & Ritsema, 1995). The temporal variation of *RR* was calculated based on the equations of Potter (1990) and the approach adopted in WEPP (Alberts et al., 1995). Initial random roughness (RR_i [cm]),that is, just after a tillage operation, is calculated according to the following equation:

$$RR_i = RR_{i\text{–tool}} f_{\text{soil}} \frac{100 + 0.5C_{\text{resi}}}{100}. \quad (3)$$

$RR_{i\text{-tool}}$ is the reference random roughness depending on the tillage implement (Alberts et al., 1995). This value is then corrected for texture effects using the soil roughness factor (f_{soil}; >1 for clay soils, 1 for silty soils, and <1 for sandy soils; USDA, 2003) and for the effects of crop residues cover (C_{resi}). Then the dynamics of *RR* over time (*t*) for a bare soil is calculated as follows:

$$RR_{\text{bare soil},t} = RR_i \, e^{-\frac{P_{cum}}{S_{stab}}}, \quad (4)$$

where P_{cum} is the cumulated rainfall since the last agricultural practice [mm] and S_{stab} is a soil structural stability parameter, estimated via the French slaking index (Rémy & Marin-Laflèche, 1974). We assumed here that *RR* for the surface covered by plant residues is not impacted by the rainfall:

$$RR_{\text{resi}} = RR_i. \quad (5)$$

A final random roughness (RR_t) can be calculated by a weighted average between RR_{resi} and $RR_{\text{bare soil},t}$ according to the cover fraction of plant residues (C_{resi}):

$$RR_t = \frac{(100 - C_{\text{resi}})RR_{\text{bare soil},t} + C_{\text{resi}}RR_{\text{resi}}}{100}. \quad (6)$$

We further assumed that *RR* remains always larger than 0.5 cm. For the deeper soil layer (25–175 cm), the Green and Ampt parameters (K_{sat2}, θ_{sat2}, ψ_2, and θ_{i2}) were assumed constant during the season (March–August 2012). K_{sat2} and θ_{sat2} were estimated with soil laboratory protocol, ψ_2 with a pedotransfer function (Saxton & Rawls, 2006) and θ_{i2} was estimated using the pF curve based on the chosen ψ_2 value (Table 2). For the topsoil layer (0–25 cm), the measured local topsoil water content (0–3 cm) could not be used directly in the model for θ_{i1} because it represents the water content of a very thin soil surface layer compared to the topsoil layer represented in LISEM (0–25 cm). θi_1 was therefore calibrated and compared with the temporal variations in measured topsoil water content and with estimations based on the soil moisture depletion model from Kohler and Linsley (1951). K_{sat1} and *n* were calibrated according to the different crops within the catchment.

The two calibration strategies were applied and developed in the following sections: (a) An event per event calibration strategy (EES) consisting in calibrating parameters independently for each runoff event as classically performed in the literature (Baartman et al., 2012; Cuomo et al., 2015; Hessel et al., 2003; Kalantari et al., 2015) and (b) a calibration with additional constraints on expected temporal evolution of K_{sat1} and *n* for the successive events (TCS).

2.4.1 | Event per Event calibration Strategy (EES)

The EES consisted in calibrating ten LISEM parameters (K_{sat1} and *n* for corn, sugar beet, wheat, and plot margins; Ψ_1 and θ_{i1}) within their physically-realistic ranges (De Roo et al., 1995; Table 2). EES was used as a reference for the evaluation of the benefits obtained with the more constrained calibration method (TCS).

2.4.2 | Temporal Constraint calibration Strategy (TCS)

To reduce the dimensionality of the parameter calibration problem and improve consistency in runoff prediction, a TCS was developed with five supplementary constraints (Table 2):

1. Ψ_1 was considered a constant because it has been shown that the Green and Ampt model could not be improved by calibrating Ψ_1 in addition to K_{sat1} (Van den Putte et al., 2013). Because LISEM is sensitive to Ψ_1 (Cuomo et al., 2015; Hessel et al., 2003), the constant value was carefully chosen and estimated with the pedotransfer function of Saxton and Rawls (2006).
2. K_{sat1} and *n* for the plot margins, such as the road, buffer strip and ditch, were fixed over time (De Roo et al., 1995) and were not calibrated because their soil surface presented less temporal variability than agricultural plots (Table 3);
3. K_{sat} for winter wheat was considered constant during the investigated period because wheat was fully developed in March and was not harvested until after the last event on July 10 (De Roo et al., 1995).
4. K_{sat} for corn and sugar beet were predicted to decrease during the growing season (Equations 7, 8, and 9), as previously observed (Van den Putte et al., 2013; Zeng et al., 2013).
5. *n* increased for winter wheat and decreased for spring-planted row crops like corn and sugar beet until mid-June (progressive surface smoothing due to aggregate degradation and crusting processes) and then increased as the vegetation tended to dominate

the resistance processes (Equation 10; O'Hare et al., 2010; Van den Putte et al., 2013).

The temporal evolution of soil saturated hydraulic conductivity ($K_{sat,t}$, [mm h^{-1}]) was determined in two steps: the saturated hydraulic conductivity of the soil matrix ($K_{sat,mtr}$) was estimated based on the pedotransfer function of Cosby, Hornberger, Clapp, and Ginn (1984), which only depends on the soil texture. The soil tillage and progressive soil clogging under the influence of rainfall were then considered (Equation 7).

$$K_{sat,t} = K_{sat,mtr} + 100(DA_{mtr} - DA_t), \tag{7}$$

where the consolidated bulk density (DA_{mtr} [g cm^{-3}]) is estimated using the pedotransfer function of Riley (1996) as a function of depth, texture, and organic matter content and the time dependent bulk density (DA_t [g cm^{-3}]). The two effects impacting DA_t are the rainfall impact and the soil tillage. For days with tillage, DA_t is estimated as follows (Equation 8):

$$DA_t = DA_{t-1} - F_p DA_{t-1} + \frac{2}{1+f_{soil}} F_p \frac{2}{3} DA_{matr}, \tag{8}$$

where DA_{t-1} is the bulk density of the previous day [g cm^{-3}] and F_p the soil fraction, which is impacted by the tillage operation. For days without tillage, the bulk density for a bare soil ($DA_{\text{bare soil},\ t}$) without residue cover is estimated by the following equation:

$$DA_{bare\ soil,\ t} = DA_{bare\ soil,t-1} + \left(DA_{matr} - DA_{bare\ soil,\ t-1}\right)\left(1 - e^{-\frac{P_j}{S_{stab}}}\right), \tag{9}$$

where P_j is the daily rainfall [mm].

The estimation of Manning's n was based on a modification of the general model $n = f$ (soil surface irregularity, obstructions, vegetation cover, and characteristics) as described by Phillips (1989) using:

$$n = n_{\text{soil}} + n_{\text{residue}} + cover \times n_{\text{veg}}. \tag{10}$$

With n_{soil} [$s/m^{1/3}$], the Manning's coefficient of bare soil, equal to one tenth of the random roughness [cm], n_{residue} [$s/m^{1/3}$] equal to 0.01 in case of less than 5% crop residue cover (which corresponds to a conventional tillage), cover fraction [−] (0 to 1), and n_{veg} equal to 0.127*crop parameter (the latter takes into account the spatial structure of the obstructions caused by the crops and was set to 0.6 for wheat, 0.3 for sugar beet, 0.15 for corn and corresponds to non-submerging overland flow and crops sowed parallel to the slope).

2.5 | Model calibration and sensitivity analysis

The calibration was focused on the outflow dynamics, that is, the observed hydrograph, at the outlet of the catchment for EES and TCS for each runoff event, except for one. For May 21, the calibration was based on the total runoff discharge volume and on the first 150 min of the hydrograph, because water storage occurred behind the dike at the outlet of the catchment and modified the natural peak flow. Limburg Soil Erosion Model calibration has often been done manually (Baartman et al., 2012; Hessel et al., 2003; Kværnø & Stolte, 2012). However, automatic calibration may help to increase prediction accuracy, to minimize modeler subjectivity, to be repeatable, and to compare more objectively two different methods of calibration with similar input parameters and different calibration settings (Doherty, 2013; Kalantari et al., 2015). The nonlinear PEST package is one of the most commonly used calibration tools in hydrological modeling and/or contaminant transport modeling problems (Bahremand & De Smedt, 2010; Kim, Benham, Brannan, Zeckoski, & Doherty, 2007; Mbonimpa et al., 2015; Wang & Brubaker, 2014). It applies a robust Gauss Marquardt Levenberg algorithm, which combines the advantages of providing fast and efficient convergence towards the minimum of the objective function that is the sum of the weighted square deviation between the measured and predicted hydrographs (Bahremand & De Smedt, 2010). Research on improving calibration results by using different PEST settings (number of adjustable parameters, range of values, weights assigned to each observations, etc) remains scarce (Doherty, 2013; Fienen, Muffels, & Hunt, 2009). Because the optimization procedure can get stuck in local minima, initial conditions to preset the model are crucial and must be accurately estimated before calibration (Cullmann, Krausse, & Saile, 2011). Understanding and controlling PEST settings would increase the probability in finding a global minimum of the objective function and dramatically decrease the calibration time compared to global calibration (Wang & Brubaker, 2014). In order to increase the probability in finding a global minimum for EES and TCS (Mbonimpa et al., 2015), the best "real" set of parameters was selected relying on measured parameters, expert knowledge, or physical laws (Table 2 and Table 3) and PEST was run to optimize input parameters within a realistic and restricted range of values (Table 2).

To assess the parameters that most significantly influenced the model results, a sensitivity analysis that varied one factor at a time was performed using the SENSAN component of PEST (Doherty, Steel, & Parrish, 2012). It was performed by increasing and decreasing each individual parameter by 20% and examining the model output in terms of total discharge. The one factor at a time method overlooks the interactions and nonlinear effects of the input parameters instead of global sensitivity analysis (Saltelli & Annoni, 2010). However, it determines the influence of the input parameters on the total discharge predictions (Sheikh et al., 2010).

2.6 | Evaluation criteria and data analysis

The predicted and observed total discharge, peak discharge, and peak time of discharge were first compared at the outlet of the catchment. The predicted and observed hydrographs were compared qualitatively (visual comparison) and quantitatively based on a multi-criteria analysis. Three criteria were calculated for comparison: (a) the Nash–Suttcliff Efficiency coefficient (*NSE*), (b) Kling–Gupta efficiency (*KGE*), and (c) the bias indicator (*BIAS*; Milella, Bisantino, Gentile, Iacobellis, & Liuzzi, 2012). The *NSE* [−] and *KGE* [−] measure how well the predicted values match the observed (Equation 11)

$$NSE = 1 - \frac{\sum_{i=1}^{n}(Q_{iobs} - Q_{isim})^2}{\sum_{i=1}^{n}\left(Q_{iobs} - \overline{Q_{obs}}\right)^2}, \tag{11}$$

where i is the time step, Q_{iobs} is the observed outflow at i, Q_{isim} is the predicted outflow at i, and $\overline{Q_{obs}}$ is the average observed outflow during the event. *KGE* (Gupta, Kling, Yilmaz, & Martinez, 2009) is estimated as follows (Equation 12):

$$KGE = 1 - \sqrt{(r-1)^2 + (\alpha-1)^2 + (\beta-1)^2}, \quad (12)$$

where r is the linear correlation coefficient between the simulated and observed discharge. α and β are determined as follows: $\alpha = \frac{\sigma_{sim}}{\sigma_{Obs}}$; $\beta = \frac{\mu_{sim}}{\mu_{Obs}}$; where σ is the standard deviation, μ is the mean value. Bias indicator measures whether the predicted values consistently over or under estimate the observed values [%] (Equation 13):

$$BIAS = 100 \times \frac{\sum_{i=1}^{n}(Q_{isim} - Q_{iobs})}{\sum_{i=1}^{n} Q_{iobs}}. \quad (13)$$

Considering the complexity of the interactions among physical processes, performing the validation at the outlet can mask important

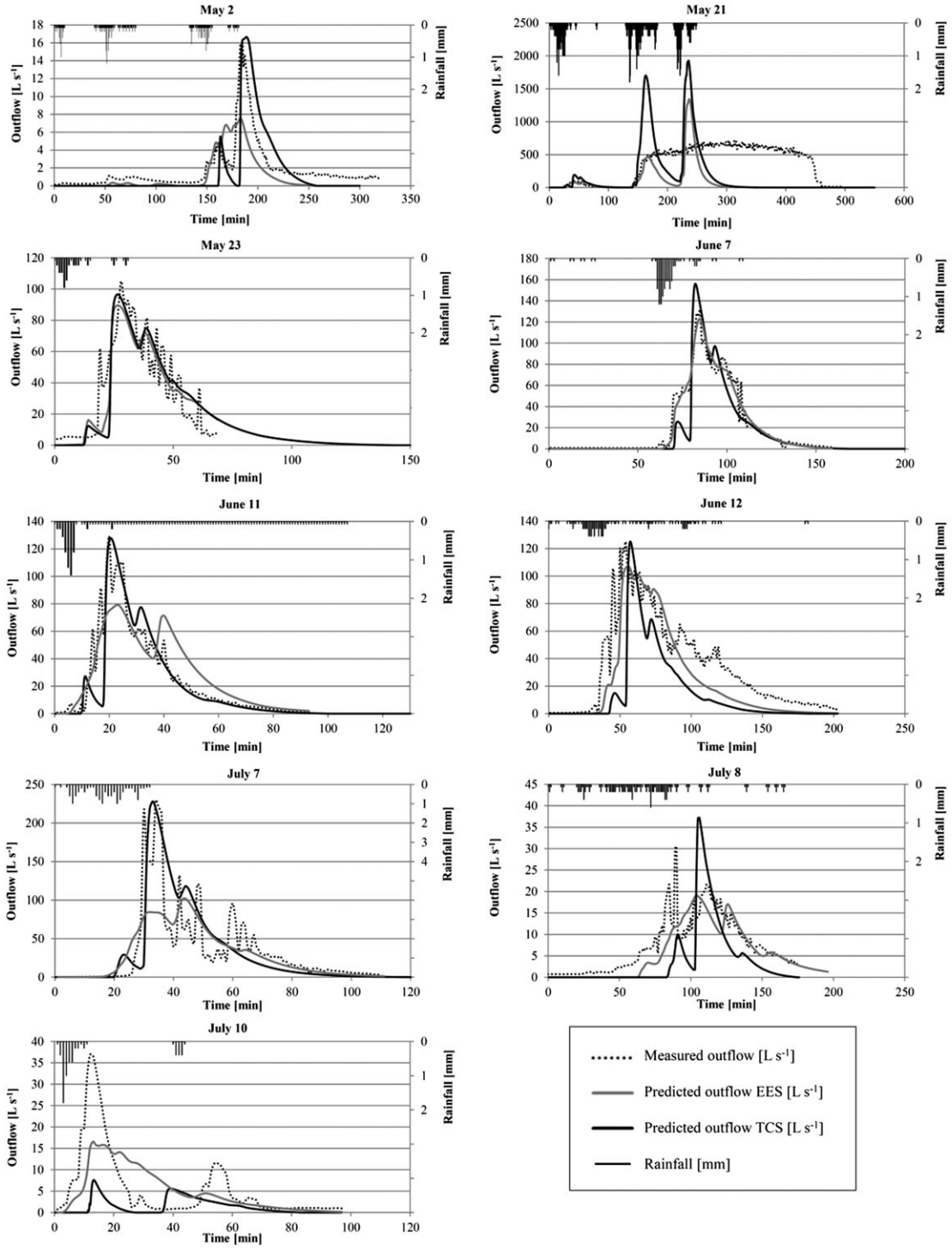

FIGURE 2 Rainfall intensity (mm mn-1), observed discharge (L s-1) together with predicted discharge according to the calibration strategies: event per event and temporal constraint strategy (EES and TCS) for the nine runoff events within the catchment (measured outflow for May 21 was hydraulically influenced by a sluice gate)

spatial variation in the catchment (Lee, Tachikawa, Sayama, & Takara, 2012). Therefore, predicted spatial runoff patterns and connectivity were compared with information collected with internal detectors (P1 and P2, Figure 1) and from direct observations on runoff traces. The calibrated parameters and their sensitivity were compared to field measurements using the paired nonparametric Wilcoxon signed rank test and the Spearman rank correlation test. Statistical tests were performed using the R software (R development Core Team, 2008; version 2.6.2).

3 | RESULTS

3.1 | Event per event calibration strategy (EES)

The observed hydrographs at the catchment outlet were predicted well by LISEM with EES (Figure 2), resulting in *NSE* and *KGE* values ranging from 0.4 to 0.97 (Table 4). On the contrary, spatial runoff patterns and connectivity were not adequately simulated, particularly for May 2 and May 21. Although observed runoff occurred at the two internal control points (P1 and P2, Figure 1) for these 2 events, only the runoff at P1 was predicted by EES. According to the LISEM predictions for the 9 runoff events, an average of 63% of the agricultural land planted in cereals triggered runoff and were hydrologically connected via surface runoff to the outlet of the catchment, whereas the field observations revealed that runoff mostly occurred on the bare soil associated with the corn and sugar beet plots (see pictures in Figure 3). For the 9 runoff events, measured total volumes were systematically under-predicted by EES, as emphasised by the negative *BIAS* values (Table 4).

As expected for the event-based calibrations (Van den Putte et al., 2013), equifinality was observed. The K_{sat1} and Ψ_1 parameters as well as the K_{sat} parameters for the different land uses compensated for each other. For example, the calibrated $K_{sat\ wheat}$ increased from 4 to 60 mm h^{-1} between June 11 and June 12, whereas in the same time period, $K_{sat\ corn}$ decreased from 60 to 6 mm h^{-1}. This is clearly unrealistic in only 1 day for an entire field.

The parameters obtained with EES were therefore highly interdependent and not consistent with agronomical knowledge. These results highlighted the weakness of calibrations performed independently for each event when temporal evolution of topsoil properties is not used as is often the case (Baartman et al., 2012; Hessel et al., 2003). The results of the TCS were then analysed in terms of spatial runoff patterns, connectivity, and dynamics compared to those obtained with the EES.

TABLE 4 Comparisons of measured and predicted runoff events with TCS in terms of total discharge [m^3], peak discharge [L s^{-1}], peak time discharge [min], and evaluation criteria (*BIAS*, *KGE*, and *NSE*) for EES and TCS approaches for each runoff event (in grey the best value between EES and TCS)

	Total discharge [m^3]			Peak discharge [L s^{-1}]			Peak time discharge [min]		
	Obs	TCS	% Diff	Obs	TCS	% Diff	Obs	TCS	% Diff
May 2	17	26.2	54.1	16	16.6	3.6	184	188.6	2.5
May 21	10411	5800.4	−44.3	[a]	1929.0	[a]	[a]	235.3	[a]
May 23	124	165.2	33.3	105	96.6	−8.7	27	26.5	−1.9
June 7	201	179.8	−10.5	131	156.0	16.0	84	82.3	−2.0
June 11	140	137.1	−2.1	129	127.8	−0.9	19	20.5	7.9
June 12	383	177.4	−53.7	125	125.1	0.1	53	57.2	7.9
July 7	217	232.6	7.2	229	228.1	−0.4	34	33.8	−0.6
July 8	69	40.0	−42.0	30	30.0	0.0	90	111.6	24.0
July 10	22	8.1	−63.2	37	7.6	−79.5	10	13.2	32.0

	BIAS (%)		*KGE* (−)		*NSE* (−)	
	EES	TCS	EES	TCS	EES	TCS
May 2	-38.87	11.30	0.45	0.55	0.57	0.02
May 21	-0.97 [b]	4.49 [b]	0.69 [b]	0.44 [b]	0.94 [b]	0.10 [b]
May 23	-2.12	-0.62	0.85	0.84	0.78	0.68
June 7	-3.31	-14.70	0.96	0.82	0.97	0.82
June 11	8.88	-7.80	0.75	0.82	0.76	0.68
June 12	-28.60	-56.45	0.70	0.35	0.73	0.21
July 7	-15.17	1.81	0.52	0.76	0.53	0.52
July 8	-19.56	-48.04	0.75	0.40	0.82	-0.01
July 10	-10.85	-75.36	0.45	-0.28	0.40	-0.17

Note. *BIAS* = bias indicator; EES = event calibration strategy; *KGE* = Kling–Gupta efficiency; *NSE* = Nash–Suttcliff efficiency; TCS = temporal constraint strategy.

[a]flood retention

[b]between the beginning of the rainfall and the flooding of the pipe

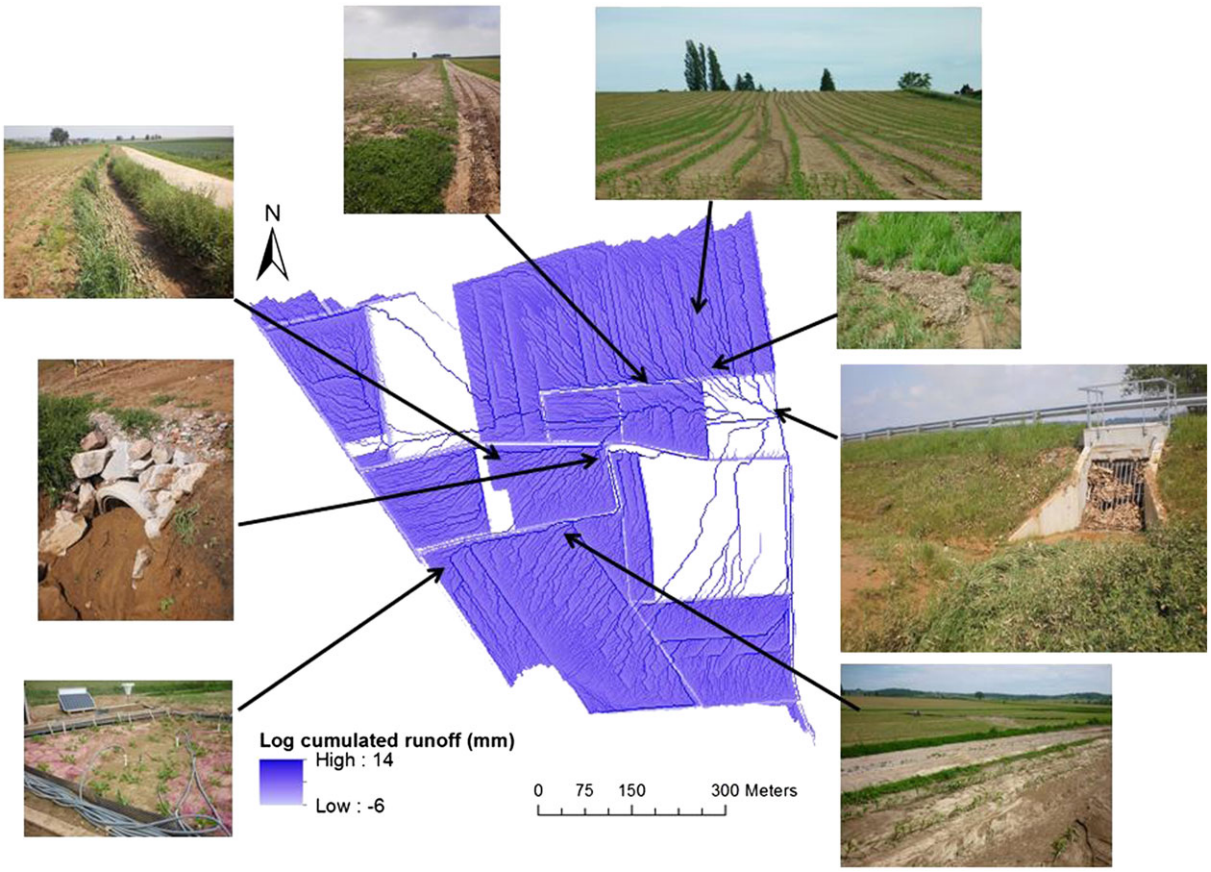

FIGURE 3 Comparison of the predicted runoff pathways for May 21 with the pictures of that day within the headwater catchment. The blue color range represents the cumulated runoff passed on each cell [log mm]

3.2 | Temporal constraint calibration strategy (TCS)

The predicted runoff dynamic at the catchment outlet was slightly degraded from EES to TCS (Table 4). The *NSE* criterion was always lower than the *NSE* criterion obtained by the EES reflecting impact of higher constraints on parameters of LISEM. The *KGE* criterion was improved only for 3 events (in grey in Table 4). For May 2 and July 10, LISEM could reproduce two peaks with the TCS compared to the EES results (Figure 2), indicating that the spatial runoff patterns and connectivity were probably better represented. Although the prediction of runoff dynamics was impacted by stronger constraints during calibration, the spatial runoff patterns and connectivity were significantly improved. Indeed, the runoff dynamics, that is, peak time and peak value, observed for the 9 events at P1 and P2 were simulated by LISEM (data not shown). Moreover, for the largest event (May 21), the predicted runoff connectivity within the catchment corresponded to the field observations (Figure 3). Fifty-four percent of the catchment surface was hydrologically connected to the outlet via surface runoff according to the LISEM runoff patterns for the 9 events studied. As observed in the field, wheat, alfalfa, and oat plots were not primary contributors to the predicted runoff with only 2% of the cereal areas connected via surface runoff. LISEM predictions showed that 50% of dirt, 35% of grass, and 100% of asphalt road surface triggered runoff in average over the 9 runoff events. Road surface (dirt, grass, and asphalt) represented 2.4% of the catchment surface, which triggered runoff, with only 1.8% hydrologically connected to the outlet. For May 2 and May 21, runoff crossed the roads to reach directly the thalweg (Figure 3) showing that the impact of slope on spatial runoff patterns was predominant against the role of the roads. The slight decrease of the *NSE* criterion based on the discharge prediction was counterbalanced by an improvement in the prediction of the runoff pathways. The associated runoff volume results were mixed with an improvement of the *BIAS* indicator for 4 events but a decrease for the others (Table 4).

The temporal variation of the calibrated value of θ_{i1} (0–25 cm) follows the same tendency as the measured topsoil water content (0–3 cm; Figure 4). The calibrated K_{sat} values varied between 0.7 and 1.5 mm h^{-1} and were in the range of values obtained in previous studies for temperate catchments with crusting soil (Risse, Nearing, & Zhang, 1995). Despite the constraint rules, a small increase of K_{sat} for corn and sugar beet values was necessary for June 7 to improve the predictions of runoff at the outlet (Figure 4). An increase of K_{sat} has been observed during an agricultural season (Mubarak et al., 2009). The need for an increase in K_{sat} on June 7 could partly be a result of the restructuring of the soil after the intensive rainfall event of May 21 and of the soil drying cycle (Mubarak et al., 2009).

3.3 | Sensitivity analysis

A sensitivity analysis was conducted for each event to quantify the impact of parameters over time on the total discharge and to invest

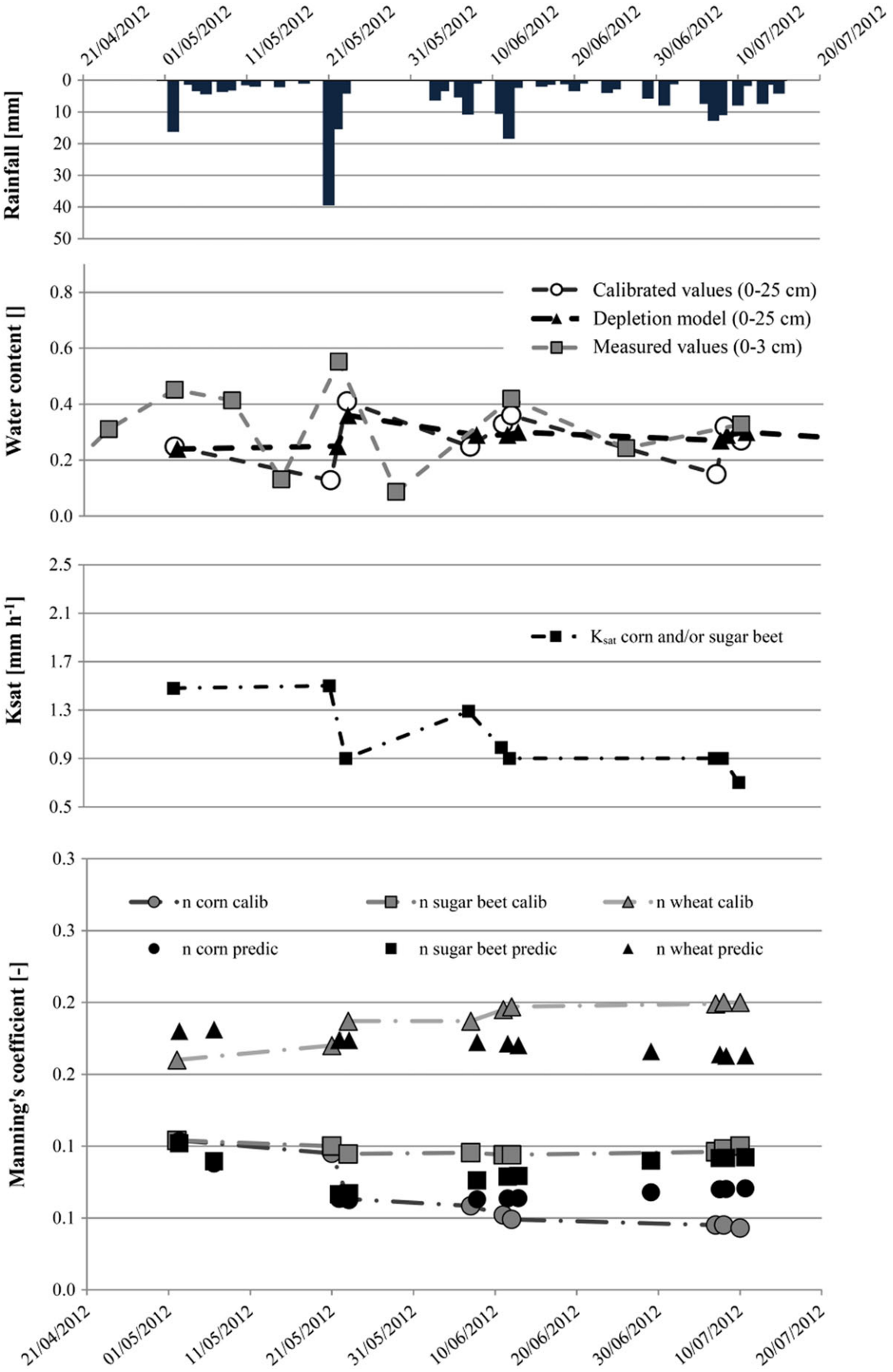

FIGURE 4 Temporal changes of initial water content, saturated hydraulic conductivity and manning coefficient related to the daily rainfall from May 2 to July 10 2012 with the TCS calibration strategy. The depletion model values for initial water content (Kohler & Linsley, 1951) and the prediction of the Manning's coefficient based on Equation 6 are represented for comparison purposes

more efforts in the calibration method focused on the most influential parameters. A sensitivity analysis of the 21 parameters of LISEM was assessed for the TCS calibrated parameters and the results are provided in Figure 5.

The results showed that the Green and Ampt parameters for the topsoil layer were the major parameters that influenced the total discharge for the 9 runoff events: in decreasing order of influence $\theta_{sat1} > \theta_{i1} > K_{sat1} > \Psi_1$ (Figure 5). This was previously shown by other authors (Sheikh et al., 2010; Zeng et al., 2013). K_{sat2}, Ψ_2, and $soildep_2$ were relatively insensitive to the total discharge (from −2 to 2% of the total discharge for 20% of the change) for the 9 runoff events (Figure 5). Those parameters would probably be more sensitive for events when excess saturation runoff occurred. Altogether, these results underlined that the in situ characterisation of soil properties has to be focused on the topsoil layer, which controls Hortonian runoff patterns in event-based models such as LISEM.

The impact of vegetation interception ranged from 0.8% of the total rainfall for the May 21 event to 19.8% for the July 10 event. This indicated that the sensitivity of the vegetation parameters increased with the vegetation growth during the season. The sensitivity of the initial moisture on the total discharge was lower (between 10 to 300 times less important) for intensive events, such as on May 21, compared to other events, which was previously shown (Sheikh et al., 2010; Hu, She, Shao, Chun, & Si, 2015). K_{sat1} was also less sensitive for runoff events with high observed runoff coefficient (p = −.98, p < .001). Altogether, these results highlight the usefulness of a multi-event sensitivity analysis to understand the temporal evolution of parameter sensitivity as field conditions change.

4 | DISCUSSION AND CONCLUSION

Potentially, physically-based models such as LISEM are best management tools to simulate impacts of changes in the catchment (land use and/or mitigation approaches) due to explicit integration of the spatial distribution of complex processes (Payraudeau & Grégoire, 2012). LISEM allows for the integration of several types of mitigation measures such as retention basins, sediment traps, vegetative barriers, or vegetative filter strips (see http://blogs.itc.nl/lisem/) and can as well simulate the effects of agronomical measures (conservation tillage, cover crops, etc.) through the appropriate modification of model parameters. However, blind EES of physically-based erosion models using measured hydrographs at the main catchment outlet may lead to an erroneous diagnosis of erosion problems within the catchment: hydrographs may be properly reproduced but simulated runoff production areas are wrong. This example of "the right answer for the wrong reason" may hamper the use of such models to define and evaluate action programs to reduce the environmental and socioeconomic impacts of overland flow and soil erosion. We have shown here that the application of a TCS of the event-based model LISEM, by using a continuous agronomic modelling approach of arable fields, yields results which properly match the observed spatial patterns of erosion and runoff source areas in the catchment. The implementation of mitigation measures in a catchment is expensive and errors in dimensioning or localising strategies can have serious economic, social, and environmental consequences and will discredit stakeholders. The TCS strategy is, therefore, an important step forward in the validation of such models for catchment management.

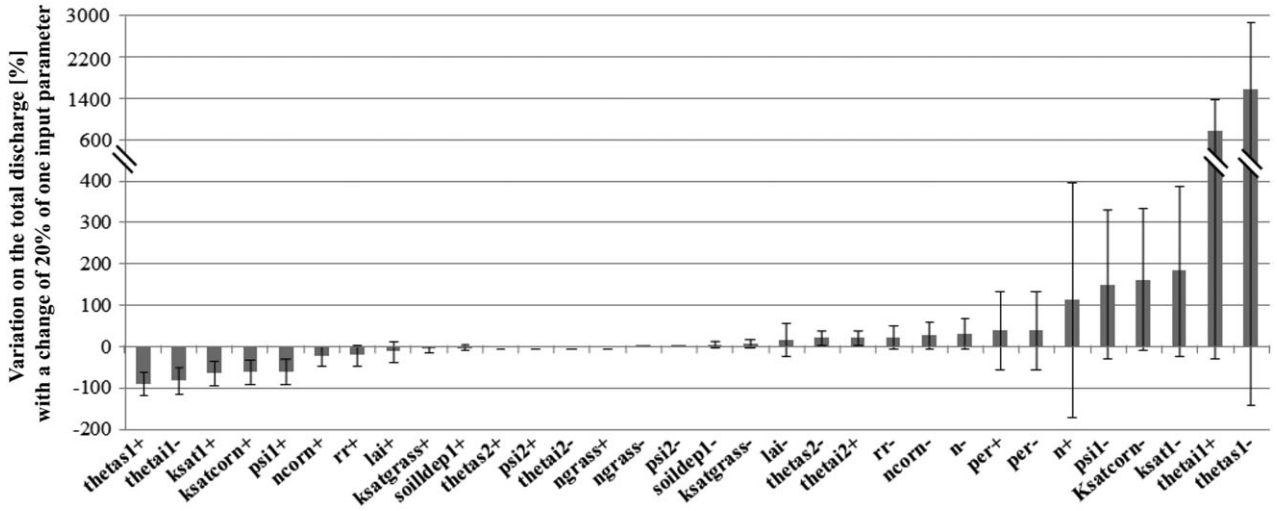

FIGURE 5 Relative sensitivity of total discharge [%] for 20% variation of each input parameter separately based on the calibrated parameters of the temporal constraint strategy (TCS). Only parameters for which total discharge sensitivity exceeded 1% were represented. Plus or minus symbol indicates 20% increase or decrease respectively. Errors bars represent the temporal variability of the sensitivity within the 9 runoff events. *Ksat1* is the saturated hydraulic conductivity of the first layer [mm h-1]; *Ksatcorn*, the saturated hydraulic conductivity for corn area [mm h-1]; *Ksatgrass*, the saturated hydraulic conductivity for grass elements (strip, ditch, track, ..) [mm h-1]; LAI, the Leaf Area Index; *n*, the Manning's coefficient; *ncorn*, the Manning's coefficient for corn area; *ngrass*, the Manning's coefficient for grass elements (strip, ditch, track, ..); *per*, the fraction of surface covered by vegetation; *rr* the random roughness [cm]; *Soildep1*, the depth of the first soil layer [cm]; $thetai_1$, the initial water content of the first soil layer; $theta_{i2}$, the initial water content for the second soil layer; $thetas_1$, the saturated water content of the first soil layer; $thetas_2$, the saturated water content for the second soil layer; psi_1, the initial soil suction of the first soil layer [cm]; psi_2, the initial soil suction of the second soil layer [cm]

Despite this improved predictive potential, modelling skills required for using these tools limit their implementation by stakeholders. Nonetheless, in the Alsace region in France the model has been applied to several catchments by the Association for Agronomic Advances in Alsace (an institution for research and development on agronomic issues) to diagnose and to evaluate the impacts of different action programs concerning the location and dimensions of sediment buffer strips and the modification of cropping systems in the area. The modelling results were successfully used by technical advisers for farmers of the Chambre d'Agriculture d'Alsace, and helped to facilitate negotiations and build consensus for remediation programs for these catchments. This example illustrates the feasibility of such a modelling approach, which provides valuable information of complex catchment responses that are difficult to assess by other means.

We have shown that several rules of calibration from TCS helped modelers to decide which parameters need to be calibrated and how. The advantages and drawbacks of TCS on spatial and temporal runoff predictions are discussed in the following part as well as its potential transfer to other catchments. Further perspectives to better estimate the spatial and temporal evolution of the two main sensitive parameters, that is, initial soil moisture and topsoil hydraulic conductivity are discussed.

4.1 | Advantages & drawbacks

This study underlined that integrating agronomical knowledge into a distributed event-based model can significantly reduce equifinality and improve the reproduction of spatial runoff patterns. With more constraints, the predicted runoff dynamic estimated by *KGE* and *NSE* criteria was slightly altered compared to a classical event per event calibration. The total discharge volume was frequently underestimated by LISEM for both strategies as indicated with a negative *BIAS* (Table 4). This could be explained by the omission of other discharge components such as subsurface flow and tile drain flow especially at the end of the event during the recession step. Despite this underestimation, the peak discharge and the peak time of discharge were correctly estimated at the outlet of the catchment but also in the 2 internal runoff detectors for the 9 runoff events (P1 and P2, Figure 1). This indicates a potential for a robust prediction of impacts of mitigation measures on runoff at the catchment scale.

The TCS method was founded on the inability to predict runoff in a cropped catchment during a growing season using a single calibration dataset. If the calibration step is not avoided with the TCS method, the calibration ranges of parameters are strongly restricted for events during the crop season. An example is given in Figure 4 where the predicted initial water content from the depletion model is very near the obtained calibrated values. Temporal constraint strategy represents a first promising step towards a full coupling between a continuous model for topsoil hydraulic properties simulation during a crop season and an event-based model.

4.2 | Transferability of the TCS method

The use of agronomical knowledge to constrain more efficiently an event-based model links the temporal evolution of key topsoil hydraulic properties with weather, soil properties, vegetation, and crop management techniques to accurately predict runoff. The constraints have to be adapted to the soil-climate-land use combination as shown by Evrard et al. (2009) in a similar approach. In terms of the scope of this application, the benefit of TCS or similar approaches may be optimal for headwater catchments with different crops with contrasting stages of vegetation from bare soil to fully covered plots. And also for soil prone to crusting such as the European loess belt (Evrard et al., 2009). The Equations 3 to 10 mathematically describe the impacts of specific crop management practices (dates, tillage implements, crop residue management, etc) on topsoil hydraulic properties and may be adapted without conceptual difficulties to different agricultural contexts. Additional relationships may be necessary in situations with significant manure applications. Indeed, contrary to mineral fertilizers, manure applications may increase soil organic carbon, field capacity, and total porosity, thus increasing the unsaturated hydraulic conductivity (Shi, Zhao, Gao, Zhang, & Wu, 2016). The equations used in this study describe the effects of organic carbon content on soil structural stability and bulk density and as a result also on the dynamics of saturated hydraulic conductivity. Effects of organic carbon content on biological activity such as earth worms are not yet integrated though they play an important role on soil meso and macroporosity and on infiltration (Alhassoun, 2009; Lamandé, Hallaire, Curmi, Pérès, & Cluzeau, 2003).

4.3 | Perspectives

The results of the sensitivity analysis provided key directions, especially regarding initial soil moisture and topsoil hydraulic properties, to improve the ability of hydrological models to predict Hortonian runoff in cropped headwater catchments during a growing season.

The sensitivity analysis highlighted an impact of initial soil moisture on runoff depending upon the intensity of rainfall events. Continuous process-based models such as CATchment HYdrology (CATHY) can provide spatiotemporal prediction of soil moisture for different soil depths. However, soil moisture prediction for crop catchments still remains challenging with this type of models due to the spatial resolution required to capture the impact of landscape components, for example, few meters to describe a grass strip (Gascuel-Odoux et al., 2009; Payraudeau & Grégoire, 2012). Since continuous models integrate processes with different dominant time scales, for example, evapotranspiration and infiltration, approaches using sub-time stepping can be a way of improving the model performance (Fatichi et al., 2016). Spatial variations of topsoil moisture can also be correctly estimated with a simple soil water balance model such as the Bridging Event and Continuous Hydrological (BEACH) model (Sheikh, Visser, & Stroosnijder, 2009) as a trade-off between parsimony and complexity. Improvement of soil moisture indices by remote sensing (Amani, Parsian, MirMazloumi, & Aieneh, 2016) or by unmanned aerial vehicles (Polo, Hornero, Duijneveld, Garcia, & Casas, 2015) can be helpful during the calibration and validation of models as shown at larger scales (Escorihuela & Quintana-Seguí, 2016).

The current limit to correctly trigger Hortonian runoff in the modelling approach is mainly due to the high spatiotemporal variability of topsoil hydraulic conductivity (Cornelissen, Diekkrüger, & Bogena, 2016; Jin et al., 2015). As discussed in the Section 1, many continuous or event-

based models do not consider the evolution of topsoil hydraulic conductivity during a growing season or use expert-based approaches with different crusting stages (Evrard et al., 2009). The integrated use of natural and virtual "laboratories" as promoted for process-based models by Fatichi et al., 2016 can be an avenue for future advances to predict the temporal evolution of topsoil hydraulic conductivity and its impact on runoff hot spots and hot-moments assessment. Thereby, measurements at plot, field, and catchment scales (Bu, Wu, & Yang, 2014; Evrard et al., 2009; Orchard, Lorentz, Jewitt, & Chaplot, 2013) and results of virtual approaches (Chahinian et al., 2006; Loague, Heppner, Ebel, & VanderKwaak, 2010) underline how agronomical and hydrological data from headwater catchments and modelling approaches can enhance the understanding and modelling of runoff processes.

ACKNOWLEDGMENTS

The authors are members of REALISE, the Network of Laboratories in Engineering and Science for the Environment in the Alsace Region (France; http://realise.unistra.fr), and the support from REALISE is gratefully acknowledged. This research was funded by the PhytoRET project (C.21) of the European INTERREG IV program in the Upper Rhine. Marie Lefrancq was supported by the European INTERREG IV program in the Upper Rhine and Water Agency of Rhine Meuse. We acknowledge, in particular, Anne-Véronique Auzet for her considerable knowledge of soil surface states, the soil laboratory UMS830 EOST/CNRS, Martine Trautmann for the soil analysis and Jean-Bernard Bardiaux for his hydraulic expertise. We would like to thank Gwenaël Imfeld for helpful comments and Richard Coupe for proof-reading the manuscript.

REFERENCES

Alhassoun, R. (2009). Studies on factors affecting the infiltration capacity of agricultural soils. Thesis, Julius Kühn-Institut Bundesforschungsinstitut für Kulturpflanzen, Quedlinburg, 156 pp.

Amani, M., Parsian, S., MirMazloumi, S. M., & Aieneh, O. (2016). Two new soil moisture indices based on the NIR-red triangle space of Landsat-8 data. *International Journal of Applied Earth Observation and Geoinformation*, *50*, 176–186.

Alberts EE, Nearing MA, Weltz MA, Risse LM, Pierson FB, Zhang XC, Laflen JM, Simanton JR. 1995. WEPP. Chapter 7. Soil component. USDA-Water Erosion Prediction Project Hillslope Profile and Watershed Model Documentation, NSERL Report 10.

Baartman, J. E. M., Jetten, V. G., Ritsema, C. J., & de Vente, J. (2012). Exploring effects of rainfall intensity and duration on soil erosion at the catchment scale using openLISEM: Prado catchment, SE Spain. *Hydrological Processes*, *26*, 1034–1049. doi:10.1002/Hyp.8196

Bahremand, A., & De Smedt, F. (2010). Predictive analysis and simulation uncertainty of a distributed hydrological model. *Water Resources Management*, *24*(12), 2869–2880. doi:10.1007/s11269-010-9584-1

Berthet, L., Andreassian, V., Perrin, C., & Javelle, P. (2009). How crucial is it to account for the antecedent moisture conditions in flood forecasting? Comparison of event-based and continuous approaches on 178 catchments. *Hydrology and Earth System Sciences*, *13*, 819–831.

Beven, K. (2006). A manifesto for the equifinality thesis. *Journal of Hydrology*, *320*, 18–36. doi:10.1016/j.jhydrol.2005.07.007

Boardman, J., & Vandaele, K. (2016). Effect of the spatial organization of land use on muddy flooding from cultivated catchments and recommendations for the adoption of control measures. *Earth Surface Processes and Landforms*, *41*, 336–343. doi:10.1002/esp.3793

Bu, C. F., Wu, S. F., & Yang, K. B. (2014). Effect of physical soil crusts on infiltration and splash erosion in three typical Chinese soils. *International Journal of Sediment Research*, *29*, 491–501.

Capowiez, Y., Cadoux, S., Bouchand, P., Roger-Estrade, J., Richard, G., & Boizard, H. (2009). Experimental evidence for the role of earthworms in compacted soil regeneration based on field observations and results from a semi-field experiment. *Soil Biology and Biochemistry*, *41*, 711–717. doi:10.1016/j.soilbio.2009.01.006

Chahinian, N., Voltz, M., Moussa, R., & Trotoux, G. (2006). Assessing the impact of the hydraulic properties of a crusted soil on overland flow modelling at the field scale. *Hydrological Processes*, *20*, 1701–1722. doi:10.1002/hyp.5948

Chow, V., Maidment, D., & Mays, L. (2013). *Applied Hydrology*, 2nd edn., McGraw-Hill Companies, Incorporated.

Chrétien, F., Gagnon, P., Thériault, G., & Guillou, M. (2016). Performance analysis of a wet-retention pond in a small agricultural catchment. *Journal of Environmental Engineering*, *142*(4). doi:10.1061/(ASCE)EE.1943-7870.0001081

Cornelissen, T., Diekkrüger, B., & Bogena, R. (2016). Using high-resolution data to test parameter sensitivity of the distributed hydrological model HydroGeoSphere. *Water*, *8*, 1–21.

Cosby, B. J., Hornberger, G. M., Clapp, R. B., & Ginn, T. R. (1984). A statistical exploration of the relationships of soil moisture characteristics to the physical properties of soils. *Water Resources Research*, *20*, 682–690. doi:10.1029/WR020i006p00682

Cullmann, J., Krausse, T., & Saile, P. (2011). Parameterising hydrological models - Comparing optimisation and robust parameter estimation. *Journal of Hydrology*, *404*, 323–331. doi:10.1016/j.jhydrol.2011.05.003

Cuomo, S., Della Sala, M., & Novita, A. (2015). Physically based modelling of soil erosion induced by rainfall in small mountain basins. *Geomorphology*, *243*, 106–115. doi:10.1016/j.geomorph.2015.04.019

De Jong, S. M., & Jetten, V. G. (2007). Estimating spatial patterns of rainfall interception from remotely sensed vegetation indices and spectral mixture analysis. *International Journal of Geographical Information Science*, *21*, 529–545. doi:10.1080/13658810601064884

De Roo, A. P. J., Wesseling, C. G., Jetten, V. G., & Ritsema, C. J. (1995). *Limburg Soil Erosion Model, A User Manual. Version 3.1. Department of Physical Geography, Utrecht University, The Winand Staring centre, Wageningen*. (pp. 48). Laon, France: The Agronomy Unit, INRA.

De Roo, A. P. J., Wesseling, C. G., & Ritsema, C. J. (1996). LISEM: A single-event physically based hydrological and soil erosion model for drainage basins .1. Theory, input and output. *Hydrological Processes*, *10*, 1107–1117.

Doherty, J. (2013). *Getting the Most Out of PEST*. Brisbane, Australia: Retrieved from http://www.pesthomepage.org/ getfiles.php?file=pest_settings.pdfWatermark Numerical Computing, QLD.

Doherty, I., Steel, C., & Parrish, D. (2012). The challenges and opportunities for professional societies in higher education in Australasia: A PEST analysis. *Australasian Journal of Educational Technology*, *28*, 105–121.

Doppler, T., Luck, A., Camenzuli, L., Krauss, M., & Stamm, C. (2014). Critical source areas for herbicides can change location depending on rain events. *Agriculture, Ecosystems & Environment*, *192*, 85–94. doi:10.1016/j.agee.2014.04.003

Escorihuela, M. J., & Quintana-Seguí, P. (2016). Comparison of remote sensing and simulated soil moisture datasets in Mediterranean landscapes. *Remote Sensing of Environment*, *180*, 99–114. doi:10.1016/j.rse.2016.02.046

Evrard, O., Cerdan, O., van Wesemael, B., Chauvet, M., Le Bissonnais, Y., Raclot, D., … Bielders, C. (2009). Reliability of an expert-based runoff and erosion model: Application of STREAM to different environments. *Catena*, *78*, 129–141. doi:10.1016/j.catena.2009.03.009

Fatichi, S., Vivoni, E. R., Ogden, F. L., Ivanov, V. Y., Mirus, B., Gochis, D., … Tarboton, D. (2016). An overview of current applications, challenges, and future trends in distributed process-based models in hydrology. *Journal of Hydrology*, *537*, 45–60. doi:10.1016/j.jhydrol.2016.03.026

Fienen, M. N., Muffels, C. T., & Hunt, R. J. (2009). On Constraining Pilot Point Calibration with Regularization in PEST. *Ground Water*, *47*, 835–844. doi:10.1111/j.1745-6584.2009.00579.x

FpMasters, B., Rohde, K., Gurner, N., & Reid, D. (2013). Reducing the risk of herbicide runoff in sugarcane farming through controlled traffic and early-banded application. *Agriculture, Ecosystems & Environment*, *180*, 29–39. doi:10.1016/j.agee.2012.02.001

Freeze, R. A., & Harlan, R. L. (1969). Blueprint for a physically-based, digitally-simulated hydrologic response model. *Journal of Hydrology*, *9*, 237–258. doi:10.1016/0022-1694(69)90020-1

Garcia-Ruiz, J. M., Nadal-Romero, E., Lana-Renault, N., & Begueria, S. (2013). Erosion in Mediterranean landscapes: Changes and future challenges. *Geomorphology*, *198*, 20–36. doi:10.1016/j.geomorph.2013.05.023

Gascuel-Odoux, C., Aurousseau, P., Cordier, M. O., Durand, P., Garcia, F., Masson, V., … Trepos, R. (2009). A decision-oriented model to evaluate the effect of land use and agricultural management on herbicide contamination in stream water. *Environmental Modelling and Software*, *24*, 1433–1446. doi:10.1016/j.envsoft.2009.06.002

Gascuel-Odoux, C., Aurousseau, P., Doray, T., Squividant, H., Macary, F., Uny, D., & Grimaldi, C. (2011). Incorporating landscape features to obtain an object-oriented landscape drainage network representing the connectivity of surface flow pathways over rural catchments. *Hydrological Processes*, *25*, 3625–3636. doi:10.1002/hyp.8089

Gupta, H. V., Kling, H., Yilmaz, K. K., & Martinez, G. F. (2009). Decomposition of the mean squared error and NSE performance criteria: Implications for improving hydrological modelling. *Journal of Hydrology*, *377*, 80–91. doi:10.1016/j.jhydrol.2009.08.003

Harel, M. A., & Mouche, E. (2014). Is the connectivity function a good indicator of soil infiltrability distribution and runoff flow dimension? *Earth Surface Processes and Landforms*, *39*, 1514–1525. doi:10.1002/esp.3604

Hasenbein, S., Lawler, S. P., Geist, J., & Connon, R. E. (2016). A Long-Term Assessment of Pesticide Mixture Effects on Aquatic Invertebrate Communities. *Environmental Toxicology and Chemistry*, *35*, 218–232. doi:10.1002/etc.3187

Heitz C, Flinois G, & Glatron S. (2012). Protection against muddy floods: Perception for local actors in Alsace (France) of a protection measure (fascines). International Disaster Risk Conference, Davos, Suisse, 26–30 Août 2012.

Her, Y., Chaubey, I., Frankenberger, J., & Smith, D. (2016). Effect of conservation practices implemented by USDA programs at field and watershed scales. *Journal of Soil and Water Conservation*, *71*, 249–266. doi:10.2489/jswc.71.3.249

Hessel, R., & Jetten, V. (2007). Suitability of transport equations in modelling soil erosion for a small Loess Plateau catchment. *Engineering Geology*, *91*, 56–71. doi:10.1016/j.enggeo.2006.12.013

Hessel, R., Messing, I., Chen, L. D., Ritsema, C., & Stolte, J. (2003). Soil erosion simulations of land use scenarios for a small Loess Plateau catchment. *Catena*, *54*, 289–302. doi:10.1016/S0341-8162(03)00070-5

Hessel, R., van den Bosch, R., & Vigiak, O. (2006). Evaluation of the LISEM soil erosion model in two catchments in the East African Highlands. *Earth Surface Processes and Landforms*, *31*, 469–486. doi:10.1002/Esp.1280

Hu, W., She, D. L., Shao, M. A., Chun, K. P., & Si, B. C. (2015). Effects of initial soil water content and saturated hydraulic conductivity variability on small watershed runoff simulation using LISEM. *Hydrological Sciences Journal*, *60*, 1137–1154. doi:10.1080/02626667.2014.903332

Hunt, R. (1982). *Plant growth curves* (Vol. 248). London: Edward Arnold.

Jin, X., Zhang, L., Gu, J., Zhao, C., Tian, J., & He, C. (2015). Modelling the impacts of spatial heterogeneity in the soil hydraulic properties on hydrological process in the upper reach of the Heihe River in the Qilian Mountains, Northwest China. *Hydrological Processes*, *29*, 3318–3327.

Kalantari, Z., Lyon, S. W., Jansson, P. E., Stolte, J., French, H. K., Folkeson, L., & Sassner, M. (2015). Modeller subjectivity and calibration impacts on hydrological model applications: An event-based comparison for a road-adjacent catchment in south-east Norway. *Science of the Total Environment*, *502*, 315–329. doi:10.1016/j.scitotenv.2014.09.030

Kamphorst, E. C., Jetten, V., Guerif, J., Pitkanen, J., Iversen, B. V., Douglas, J. T., & Paz, A. (2000). Predicting depressional storage from soil surface roughness. *Soil Science Society of America Journal*, *64*, 1749–1758.

Kim, S. M., Benham, B. L., Brannan, K. M., Zeckoski, R. W., & Doherty, J. (2007). Comparison of hydrologic calibration of HSPF using automatic and manual methods. *Water Resources Research*, *43*, W01402. doi:10.1029/2006WR004883

Kirchner, J. W. (2006). Getting the right answers for the right reasons: Linking measurements, analyses, and models to advance the science of hydrology. *Water Resources Research*, 42. doi:10.1029/2005wr004362

Kohler MA, & Linsley RK. (1951). Predicting the runoff from storm rainfall. US weather Bureau Res.

Kutílek, M., & Nielsen, D. R. (1994). *Soil hydrology*. Cremlingen-Destedt, Germany: Catena Verlag.

Kværnø, S. H., & Stolte, J. (2012). Effects of soil physical data sources on discharge and soil loss simulated by the LISEM model. *Catena*, *97*, 137–149. doi:10.1016/j.catena.2012.05.001

Lamandé, M., Hallaire, V., Curmi, P., Pérès, G., & Cluzeau, D. (2003). Changes of pore morphology, infiltration and earthworm community in a loamy soil under different agricultural managements. *Catena*, *54*, 637–649. doi:10.1016/S0341-8162(03)00114-0

Lee, G., Tachikawa, Y., Sayama, T., & Takara, K. (2012). Catchment responses to plausible parameters and input data under equifinality in distributed rainfall-runoff modeling. *Hydrological Processes*, *26*, 893–906. doi:10.1002/Hyp.8303

Levavasseur, F., Bailly, J. S., Lagacherie, P., Colin, F., & Rabotin, M. (2012). Simulating the effects of spatial configurations of agricultural ditch drainage networks on surface runoff from agricultural catchments. *Hydrological Processes*, *26*, 3393–3404. doi:10.1002/hyp.8422

Li, Z., & Zhang, J. T. (2001). Calculation of field Manning's roughness coefficient. *Agricultural Water Management*, *49*, 153–161. doi:10.1016/S0378-3774(00)00139-6

Liu, G. B., Xu, M. X., & Ritsema, C. (2003). A study of soil surface characteristics in a small watershed in the hilly, gullied area on the Chinese Loess Plateau. *Catena*, *54*, 31–44. doi:10.1016/S0341-8162(03)00055-9

Loague, K., Heppner, C. S., Ebel, B. A., & VanderKwaak, J. E. (2010). The quixotic search for a comprehensive understandong of hydrologic response at the surface: Horton, Dunne, Dunton, and the role of concept-development simulation. *Hydrological Processes*, *24*, 2499–2505.

Madsen, H.B., Jensen, C.R., & Boysen, T. (1986). A comparison of the thermocouple psychrometer and the pressure plate methods for determination of soil-water characteristic curves. *Journal of Soil Science*, *37*, 357–362. doi: 10.1111/j.1365-2389.1986.tb00368.x

Master, B., Rohde, K., Gurner, N., & Reid, D. (2013). Reducing the risk of herbicide runoff in sugarcane farming through controlled traffic and early-banded application. *Agricuture, Ecosystems and Environment*, *180*, 29–39. doi:10.1016/j.agee.2012.02.001

Mbonimpa, E. G., Gautam, S., Lai, L., Kumar, S., Bonta, J. V., Wang, X., & Rafique, R. (2015). Combined PEST and Trial–Error approach to improve APEX calibration. *Computers and Electronics in Agriculture*, *114*, 296–303. doi:10.1016/j.compag.2015.04.014

McCuen, R.H., 2004. Hydrologic analysis and design. Prentice Hall, Upper Saddle River, New Jersey, ISBN-0-13-142424-6.

Milella, P., Bisantino, T., Gentile, F., Iacobellis, V., & Liuzzi, G. T. (2012). Diagnostic analysis of distributed input and parameter datasets in Mediterranean basin streamflow modeling. *Journal of Hydrology*, *472*, 262–276. doi:10.1016/j.jhydrol.2012.09.039

Mubarak, I., Mailhol, J. C., Angulo-Jaramillo, R., Ruelle, P., Boivin, P., & Khaledian, M. (2009). Temporal variability in soil hydraulic properties under drip irrigation. *Geoderma*, *150*, 158–165. doi:10.1016/j.geoderma.2009.01.022

Muma, M., Gumiere, S. J., & Rousseau, A. N. (2014). Comprehensive analysis of the CATHY model sensitivity to soil hydrodynamic properties of a tile-drained, agricultural micro-watershed. *Hydrological Sciences Journal*, *59*, 1606–1623. doi:10.1080/02626667.2013.843778

O'Hare, M. T., McGahey, C., Bissett, N., Cailes, C., Henville, P., & Scarlett, P. (2010). Variability in roughness measurements for vegetated rivers near base flow, in England and Scotland. *Journal of Hydrology*, *385*, 361–370. doi:10.1016/j.jhydrol.2010.02.036

Orchard, C. M., Lorentz, S. A., Jewitt, G. P. W., & Chaplot, V. A. M. (2013). Spatial and temporal variations of overland flow during rainfall events and in relation to catchment conditions. *Hydrological Processes*, *27*, 2325–2338. doi:10.1002/hyp.9217

Outram, F. N., Cooper, R. J., Sunnenberg, G., Hiscock, K. M., & Lovett, A. A. (2016). Antecedent conditions, hydrological connectivity and anthropogenic inputs: Factors affecting nitrate and phosphorus transfers to agricultural headwater streams. *Science of the Total Environment*, *545*, 184–199. doi:10.1016/j.scitotenv.2015.12.025

Pandey, A., Himanshu, S. K., Mishra, S. K., & Singh, V. P. (2016). Physically based soil erosion and sediment yield models revisited. *Catena*, *147*, 595–620. doi:10.1016/j.catena.2016.08.002

Pare, N., Andrieux, P., Louchart, X., Biarnes, A., & Voltz, M. (2011). Predicting the spatio-temporal dynamic of soil surface characteristics after tillage. *Soil & Tillage Research*, *114*, 135–145. doi:10.1016/j.still.2011.04.003

Payraudeau, S., & Grégoire, C. (2012). Modelling pesticides transfer to surface water at the catchment scale: a multi-criteria analysis. *Agronomy for Sustainable Development*, *32*, 479–500. doi:10.1007/s13593-011-0023-3

Phillips, J. D. (1989). Predicting minimum achievable soil loss in developing-countries. *Applied Geography*, *9*, 219–236. doi:10.1016/0143-6228(89)90025-8

Polo, J., Hornero, G., Duijneveld, C., Garcia, A., & Casas, O. (2015). Design of a low-cost wireless sensor network with UAV mobile node for agricultural applications. *Computers and Electronics in Agriculture*, *119*, 19–32.

Potter, K. N. (1990). Soil properties effect on random roughness decay by rainfall. *Transactions of the Asae*, *33*, 1889–1892.

R Development Core Team (2008). R: A language and environment for statistical computing. R Foundation for Statistical Computing, Vienna, Austria ISBN 3-900051-07-0, URL http://www.R-project.org.

Rémy, J. C., & Marin-Laflèche, A. (1974). L'analyse de terre : réalisation d'un programme d'interprétation automatique. *Annales Agronomiques*, *25*(4), 607–632.

Riley, H. (1996). Estimation of physical properties of cultivated soils in southeast Norway from readily available soil information Norwegian. *Journal of Agricultural Science*, *25*, 1–51.

Risse, L. M., Nearing, M. A., & Zhang, X. C. (1995). Variability in Green-Ampt effective hydraulic conductivity under fallow conditions. *Journal of Hydrology*, *169*, 1–24. doi:10.1016/0022-1694(94)02676-3

Rodriguez-Caballero, E., Canton, Y., & Jetten, V. (2015). Biological soil crust effects must be included to accurately model infiltration and erosion in drylands: An example from Tabernas Badlands. *Geomorphology*, *241*, 331–342. doi:10.1016/j.geomorph.2015.03.042

Saltelli, A., & Annoni, P. (2010). How to avoid a perfunctory sensitivity analysis. *Environmental Modelling and Software*, *25*, 1508–1517. doi:10.1016/j.envsoft.2010.04.012

Saxton, K. E., & Rawls, W. J. (2006). Soil water characteristic estimates by texture and organic matter for hydrologic solutions. *Soil Science Society of America Journal*, *70*, 1569–1578. doi:10.2136/sssaj2005.0117

Sheikh, V., Visser, S., & Stroosnijder, L. (2009). A simple model to predict soil moisture: Bridging Event and Continuous Hydrological (BEACH) modelling. *Environmental Modelling and Software*, *24*, 542–556. doi:10.1016/j.envsoft.2008.10.005

Sheikh, V., van Loon, E., Hessel, R., & Jetten, V. (2010). Sensitivity of LISEM predicted catchment discharge to initial soil moisture content of soil profile. *Journal of Hydrology*, *393*, 174–185. doi:10.1016/j.jhydrol.2010.08.016

Shi, Y., Zhao, X., Gao, X., Zhang, S., & Wu, P. (2016). The effects of long-term fertiliser applications on soil organic carbon and hydraulic properties of a loess soil in China. *Land Degradation and Development*, *27*, 60–67. doi:10.1002/ldr.2391

Smith, R. E., & Parlange, J.-Y. (1978). A parameter-efficient hydrologic infiltration model. *Water Resources Research*, *14*, 533–538.

Starkloff, T., & Stolte, J. (2014). Applied comparison of the erosion risk models EROSION 3D and LISEM for a small catchment in Norway. *Catena*, *118*, 154–167. doi:10.1016/j.catena.2014.02.004

Thomas, I. A., Jordan, P., Shine, O., Fenton, O., Mellander, P.-E., Dunlop, P., & Murphy, P. N. C. (2017). Defining optimal DEM resolutions and point densities for modelling hydrologically sensitive areas in agricultural catchments dominated by microtopography. *International Journal of Applied Earth Observation and Geoinformation*, *54*, 38–52. doi:10.1016/j.jag.2016.08.012

Tramblay, Y., Bouvier, C., Martin, C., Didon-Lescot, J. F., Todorovik, D., & Domergue, J. M. (2010). Assessment of initial soil moisture conditions for event-based rainfall-runoff modelling. *Journal of Hydrology*, *387*, 176–187. doi:10.1016/j.jhydrol.2010.04.006

USDA. (2003). Revisited Universal Soil Loss Equation. Version 2. RUSLE2.

Van den Putte, A., Govers, G., Leys, A., Langhans, C., Clymans, W., & Diels, J. (2013). Estimating the parameters of the Green-Ampt infiltration equation from rainfall simulation data: Why simpler is better. *Journal of Hydrology*, *476*, 332–344. doi:10.1016/j.jhydrol.2012.10.051

Wang, Y., & Brubaker, K. (2014). Implementing a nonlinear groundwater module in the soil and water assessment tool (SWAT). *Hydrological Processes*, *28*, 3388–3403. doi:10.1002/hyp.9893

Yin, Y. X., Jiang, S. Y., Pers, C., Yang, X. Y., Liu, Q., Yuan, J., … Zheng, Z. (2016). Assessment of the spatial and temporal variations of water quality for agricultural lands with crop rotation in China by using a HYPE Model. *International Journal Environmental Research Pub He*, *13*. doi:10.3390/ijerph13030336

Zeng, C., Wang, Q. J., Zhang, F., & Zhang, J. (2013). Temporal changes in soil hydraulic conductivity with different soil types and irrigation methods. *Geoderma*, *193*, 290–299. doi:10.1016/j.geoderma.2012.10.013

Zhang, D., Madsen, H., Ridler, M. E., Refsgaard, J. C., & Jensen, K. H. (2015). Impact of uncertainty description on assimilating hydraulic head in the MIKE SHE distributed hydrological model, Adv. *Water Resources*, *86*, 400–413. doi:10.1016/j.advwatres.2015.07.018

How to cite this article: Lefrancq M, Van Dijk P, Jetten V, Schwob M, Payraudeau S. Improving runoff prediction using agronomical information in a cropped, loess covered catchment, *Hydrological Processes*. 2017;**31:**1408–1423. https://doi.org/10.1002/hyp.11115